Characterization of submicron aerosol chemical composition and sources in the coastal area of Central Chile

Saarikoski, S.

2019-02-15

Saarikoski , S , Reyes , F , Vázquez , Y , Tagle , M , Timonen , H , Aurela , M , Carbone , S , Worsnop , D R , Hillamo , R & Oyola , P 2019 , ' Characterization of submicron aerosol chemical composition and sources in the coastal area of Central Chile ' , Atmospheric Environment , vol. 199 , pp. 391-401 . https://doi.org/10.1016/j.atmosenv.2018.11.040

http://hdl.handle.net/10138/298815
https://doi.org/10.1016/j.atmosenv.2018.11.040

Atmospheric Environment 199 (2019) 391–401

Contents lists available at ScienceDirect

Atmospheric Environment

journal homepage: www.elsevier.com/locate/atmosenv

Characterization of submicron aerosol chemical composition and sources in the coastal area of Central Chile

S. Saarikoski[a,*], F. Reyes[b], Y. Vázquez[b], M. Tagle[b], H. Timonen[a], M. Aurela[a], S. Carbone[a,c], D.R. Worsnop[a,d,e], R. Hillamo[a], P. Oyola[b]

[a] Atmospheric Composition Research, Finnish Meteorological Institute, FI-00101, Helsinki, Finland
[b] Centro Mario Molina Chile, 7510121, Santiago, Chile
[c] Institute of Agrarian Sciences, Federal University of Uberlandia, Uberlandia, Brazil
[d] Aerodyne Research, Billerica, MA, 01821-3976, USA
[e] Department of Physics, University of Helsinki, FI-00014, Helsinki, Finland

ARTICLE INFO

Keywords:
Submicron particles
Chemical composition
Aerosol Mass Spectrometer
Source apportionment
South America

ABSTRACT

Chemical characteristics and the sources of submicron particles (< 1 μm in diameter) were investigated in Valle Alegre, the coastal area of Central Chile. The chemical composition of particles was studied by using a Soot particle Aerosol Mass Spectrometer and Multi-Angle Absorption Photometer. Submicron particles were dominated by organics (42% of mass) and sulfate (39% of mass) while the mass fractions of ammonium, nitrate and black carbon were much smaller (13, 2 and 4% of mass, respectively). Additionally, several metals (V, Zn, Fe, Cd, Cu, K, Na and Mg) were detected in submicron particles and also some of their inorganic salts (e.g. $NaCl^+$, $MgCl_2^+$, $CaCl_2^+$, KCl^+ and KNO_3^+). The sources of particles were examined by using Positive Matrix Factorization (PMF). Organic aerosol (OA) was divided into five factors by using PMF; hydrocarbon-like OA (HOA), biomass burning OA (BBOA), low-volatility oxygenated OA (LV-OOA), semi-volatile OA (SV-OOA) and marine oxygenated OOA (MOOA). Oxygenated factors (LV-OOA; SV-OOA and MOOA) comprised 75% of total OA with LV-OOA being the dominant factor (38% of OA). Sulfate had two major sources in Valle Alegre; ~70% of sulfate was related to anthropogenic sources through the oxidation of gas phase SO_2 whereas ~24% of sulfate was associated with biogenic origin related to the oxidation of dimethyl sulfide in the marine environment. Regarding total submicron particle mass (campaign-average 9.5 μg m^{-3}), the contribution of anthropogenic sources was at least as large as that of biogenic origin.

1. Introduction

Global Burden of Disease studies have shown that the exposure to ambient particulate matter (PM) with aerodynamic diameter < 2.5 μm ($PM_{2.5}$) is among the top ten risks faced by human beings today (WHO, 2016a; 2016b). On the global level, the exposure to outdoor air pollution, mostly to PM, causes 3.3 million premature deaths per year (Lelieveld et al., 2015). The relative contributions of different emission sources vary significantly but e.g. in densely populated western countries, 33–55% of premature deaths caused by air pollution are related to anthropogenic aerosol. In addition to adverse health effects, anthropogenic particles influence on climate. Due to their complex physical and chemical properties, atmospheric aerosols still cause the largest uncertainty to the total radiative forcing estimate (IPCC, 2013).

Sources of anthropogenic pollution have mostly been investigated in urban areas with rather well-known pollution sources such as traffic, residential burning (biomass/coal), cooking and energy production (e.g. Aiken et al., 2009; He et al., 2011; Elser et al., 2016). In rural areas, the contribution of biogenic sources is typically larger but also anthropogenic sources can be more diverse and significantly different from urban areas (Kortelainen et al., 2017). In rural locations, ambient particles can be e.g. strongly influenced by industrial sources as industrial activities are often situated near small towns or in sparsely populated areas. In case of industrial sources, emissions from point sources, such as from stacks, are usually regulated and the emissions can be determined by standard methods but there are also a lot of fugitive emissions that are much more difficult to control and quantify. Ideally, industrial facilities would be located far away from habitation, in order to minimize their air quality impact, but in most cases that is unfeasible because of the need of labor and efficient transportation

* Corresponding author. Finnish Meteorological Institute, P.O.Box 503, FI-00101, Helsinki, Finland.
E-mail address: Sanna.Saarikoski@fmi.fi (S. Saarikoski).

https://doi.org/10.1016/j.atmosenv.2018.11.040
Received 18 May 2018; Received in revised form 14 November 2018; Accepted 16 November 2018
Available online 22 November 2018

system.

Chile is one of the countries suffering from air pollution episodes (Gramsch et al., 2006, 2016). In the past, the capital of Chile, Santiago, was one of the most polluted cities in the world, but due to the successful pollution control plan, the concentrations of air pollutants have been reduced (Koutrakis et al., 2005). Nowadays submicron particle mass concentrations in Santiago are not higher than in some other large cities (e.g. Huang et al., 2011; Carbone et al., 2013; Sun et al., 2015; Gramsch et al., 2016; Tagle et al., 2018). As Chile is wealth in minerals, mostly copper, it is one of the most highly industrialized Latin American countries. Currently, Chile has serious air quality concerns in rural areas where a large number of industrial activities are situated.

The largest industrial region in Chile is the Santiago-Valparaíso area. Valle Alegre is a rural valley in Valparaiso Region with a lot of agricultural activity but there is also a large industrial area with e.g. smelters, power plants, oil refineries and cement factories nearby. The industrial site also incorporates one of the most important port activities in the region. The area has been officially recognized by the state of Chile as "Saturated Area" for $PM_{2.5}$ which means that mass concentrations exceed the national air quality standard for $PM_{2.5}$ (annual limit of 20 $\mu g\,m^{-3}$) and "Latent area" for PM_{10} which means concentration are close to the national air quality standard (over 80% of the annual limit of 50 $\mu g\,m^{-3}$).

The aim of this study was to investigate the chemical characteristics and sources of submicron particles in Valle Alegre by using a Soot particle Aerosol Mass Spectrometer (SP-AMS). The SP-AMS enables the detection of non-refractory aerosol species (organics, sulfate, nitrate, ammonium and chloride) and refractory material e.g. refractory black carbon (rBC) and metals. In order to examine the sources of particles in Valle Alegre, Positive Matrix Factorization (PMF) was applied to the mass spectra (MS) of organic aerosol (OA). In addition to OA, PMF was also utilized unconventionally by adding sulfate fragments to the OA data matrix to examine the origin of sulfate in Valle Alegre. The specific objective of this study was to assess the impact of anthropogenic and biogenic sources to particulate pollution. Although the sources and chemistry of submicron particles have been investigated extensively around the world, until now most of the studies have been carried out in the northern hemisphere. In the southern hemisphere, there are still areas that are lacking information related to local air quality and climate change that can be different from the northern hemisphere. To our knowledge, this is the most extensive study characterizing the chemical properties of submicron particles in the rural area of Central Chile.

2. Experimental methods

2.1. Measurement site and period

Measurement site was located in Valle Alegre in Central Chile (32°48′28.24"S, 71°26′12.85"W; Fig. 1a). Valle Alegre is a rural valley ~7 km inland from the bay of Quintero enclosed by the coastal mountain range at the east side. It is situated ~12 kilometers away from one of the largest industrial complex in Chile, Ventanas. The industrial park comprises a 5-terminal port and 14 industrial facilities: four coal-fired power plants, one copper sulfate smelter, one copper refinery, three gas and diesel storage facilities, two petrochemical factories, and two industries processing asphalt and cement. The industrial sites are mostly located north-west from the station, at the Pacific coast. Five largest industrial sites in the region are shown in Fig. 1a.

The measurements were carried out from 9 to 28 January 2015 (austral summer). Instruments were placed in a container at a corner of a private recreation area with some outdoor activities (e.g. pool, barbecue area). However, as the recreational area was still partially under construction, there was not much recreational or building activity during the measurement campaign. The other side on the container was bordered by a small forest. There was also some agricultural activity near the site as well as cattle and horses.

2.2. Instruments

2.2.1. Soot Particle Aerosol Mass Spectrometer

The chemical composition of submicron particles was measured by using a Soot Particle Aerosol Mass Spectrometer (Aerodyne Research Inc., Billerica, USA; Onasch et al., 2012). The SP-AMS is a high resolution Time-of-Flight aerosol mass spectrometer (HR-ToF-AMS; DeCarlo et al., 2006) that has an additional laser vaporizer. The SP-AMS is able to measure non-refractory species (organics, sulfate, nitrate, ammonium and chloride) but also rBC and some metals due to the laser vaporizer (ND:YAG 1064 nm). Typically, the SP-AMS operates in two modes, MS mode, in which the chemical composition of all particles in the size range of the instrument (~50–800 nm) is measured, and efficient Particle-time-of flight (ePToF) mode that allows the determination of chemical species as a function of particle size. In the MS mode, the chopper is alternated between open and closed positions of which open allows the particle beam to pass through and closed blocks it. In the ePToF mode, the chopper is continuously rotating (~140 Hz) and as it has several slits that let the particle beam pass through. The SP-AMS data was recorded with one minute time-resolution of which half of the time the SP-AMS measured in the MS and half in the ePToF mode. The SP-AMS was equipped with both tungsten vaporizer (at 600 °C) and laser vaporizer. Typically, the SP-AMS operates by switching the laser on and off, however, during this campaign there was a malfunction with the laser power. Therefore, the laser was on continuously from 9 to 18 January after which the laser was off for the rest of the campaign. The SP-AMS had a cyclone (SCC 1.828, BGI Inc., US) in the sample line outside the container in order to remove particles larger than 1 μm in diameter from the sample flow.

2.2.2. Multi Angle Absorption Photometer

A Multi-Angle Absorption Photometer (MAAP, Model 5012, Thermo Fisher Scientific, Waltham, USA) was used to determine the concentration of black carbon (BC). In the MAAP, particles are deposited on a quartz fiber filter and a continuous laser beam (670 nm) is passed perpendicular through the filter. The decrease in the transmitted light is due to two factors; absorption by the particles on the filter and scattering by the particles and filter matrix. Absorbance of the particles is determined by subtracting scattering, measured by the additional detectors placed at selected angles, from the decrease in the light intensity (Petzold and Schönlinner, 2004). In this study, a default mass-specific aerosol absorption coefficient (σ_{abs}) of 6.6 $m^2\,g^{-1}$ was used for the MAAP results. The data averaging time was one minute and the flow rate was 11 lpm. The MAAP had an inlet with the 50% cut-off at 1 μm placed outside the container. The comparison between rBC from the SP-AMS and BC from the MAAP is presented in Supplementary material (Fig. S1). The time series of rBC and BC followed similar trend but overall their correlation was rather poor. BC results presented in this article are mostly obtained from the MAAP. Only for the size-distribution of BC the results are taken from the SP-AMS but in that case the corresponding species is referred as rBC.

2.2.3. Air quality measurements, meteorology and backward trajectories

An air quality monitoring station operated by local industrial companies was situated next to the measurement container. Hourly averaged PM_{10} concentration was measured with Continuous Ambient Particulate Monitor (FH62C14, Thermo Fisher Scientific, Waltham, USA), nitrogen oxides with NO-NO_2-NO_x Analyzer (42*i*, Thermo Fisher Scientific, Waltham, USA), sulfur dioxide (SO_2) with SO_2 Analyzer (43*i*, Thermo Fisher Scientific, Waltham, USA) and ozone (O_3) with Ozone Analyzer (49*i*, Thermo Fisher Scientific, Waltham, USA). Unfortunately, there were neither $PM_{2.5}$ nor PM_1 measurement at the air quality monitoring station. Meteorological parameters (temperature, wind direction and wind speed) were monitored with Met One Sensors (Met One Instruments Inc, Grants Pass, USA), however, due to the malfunctioning of the temperature sensor in Valle Alegre, temperature was

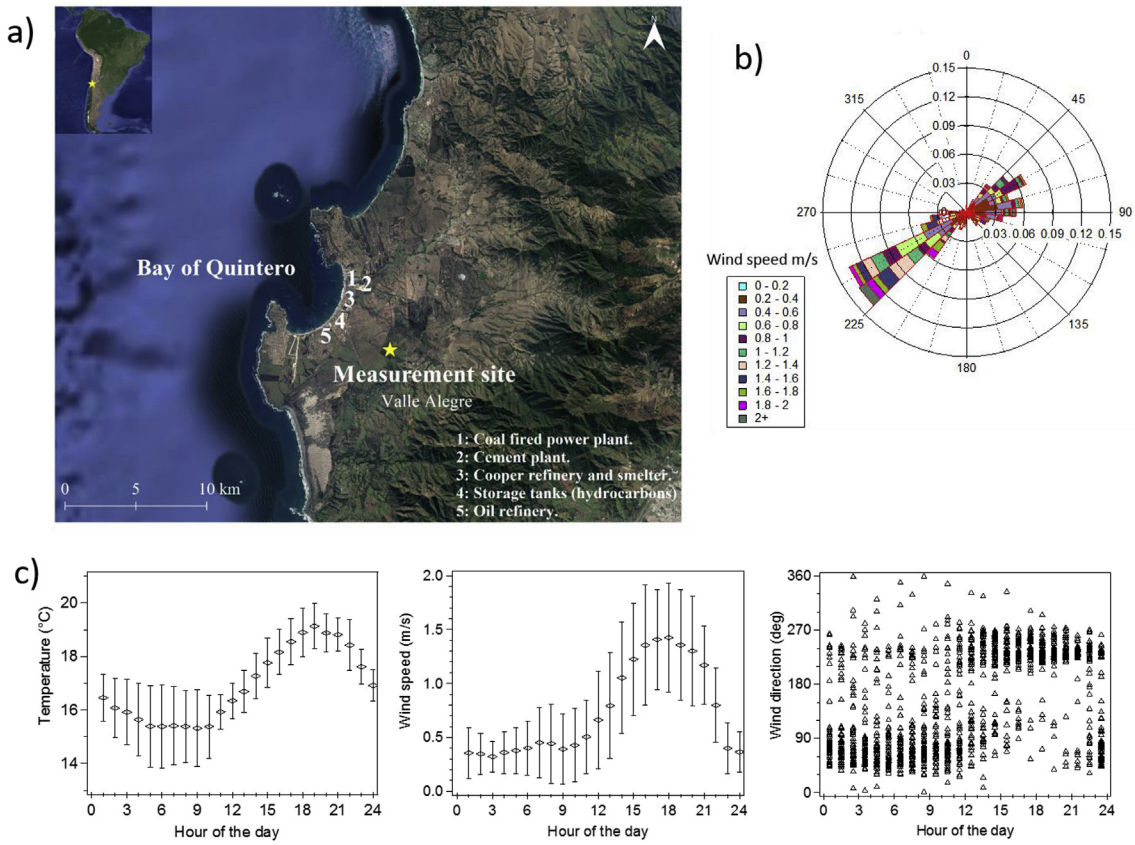

Fig. 1. The location of the measurement site in Valle Alegre, Chile (a), the average wind direction pattern at the site (b), and the diurnal variation of meteorological parameters (c). Temperature and wind speed are presented as average ± stdev while in wind direction plot individual (hourly) values are shown. Temperature in (c) was obtained from the air quality monitoring station in Quintero ~10 km from the Valle Alegre station.

obtained from the air quality monitoring station in Quintero (~10 km from Valle Alegre station).

72-h air mass backward trajectories were calculated in order to investigate the origin and transport history of air masses that arrived in Valle Alegre. Trajectories were calculated by using the NOAA Hybrid Single-Particle Lagrangian Integrated Trajectory model (Draxler and Rolph, 2003; Stein et al., 2015) and global meteorological data from the Global Data Assimilation System (GDAS) archive with an arrival height of 500 m above the ground. Trajectories were calculated every 3 h for the period of 9–28 January 2015.

2.3. Laboratory measurements for reference mass spectra

Reference mass spectra for methane sulfonic acid (MSA) and ammonium sulfate were obtained by laboratory tests. MSA and ammonium sulfate standards were dissolved in Milli-Q water, and particles were produced by an aerosol generator (Model 3076, TSI Inc., Shoreview, USA). 300 nm particles were selected with the Differential Mobility Analyzer (DMA; Model 3082, TSI Inc., Shoreview, USA) and directed to the SP-AMS.

2.4. Data analysis

2.4.1. Relative ionization efficiency and collection efficiency for the SP-AMS

The SP-AMS data was analyzed with Igor 6.3 software using SQRL 1.56D and PIKA 1.15D. Elemental analysis of OA was accomplished with the method developed originally by Aiken et al. (2007, 2008) but extended to a wider range of OA species by Canagaratna et al. (2015). The ionization efficiency (IE) of nitrate was determined by calibrating the instrument by using monodisperse ammonium nitrate particles. Default relative ionization efficiencies (RIEs) were used for organics and chloride whereas for sulfate and ammonium the RIEs of 0.86 and 3.1 were used, respectively, based on the ammonium sulfate and ammonium nitrate calibrations carried out in the laboratory. For rBC, the RIE of 0.1 was obtained from the calibration with Regal black. For metals, the RIEs were taken from the study of Carbone et al. (2015). Since the exact RIE was not available for Cd, K and Mg, a default RIE of 1 was used for them. By using the values given in Carbone et al. (2015), it was assumed that metals were in the same particles with rBC. However, that may not always be true, especially in Valle Alegre where the sources of metals and rBC can be quite different. Mg and Zn were determined as their isotopes at m/z 25 ($^{25}Mg^+$) and 68 ($^{68}Zn^+$), respectively, as the main isotopes were overlapped by SO^{++} (at m/z 24) and SO_2^+ (at m/z 64) fragments. Size distribution (ePToF) data was analyzed only with unit mass resolution (UMR) because the tool for the high resolution ePToF data was not available.

The collection efficiency (CE) was calculated according to Middlebrook et al. (2012). Most of the time the CE was 0.45, which is the lower limit of the CE based on the equation of Middlebrook et al. (2012), but there were several events when the CE was as large as 0.8 (see Fig. S2). During those periods particles were acidic due to the larger amount of sulfate compared to that of ammonium. Relative humidity was not measured continuously from the sample air, and therefore, that could not be taken into account when calculating the CE. It should be noted that for the SP-AMS the CE can be different from the standard AMS due to the additional laser vaporizer. The factors affecting the CE in the SP-AMS have been discussed e.g. in Onasch et al. (2012), Willis et al. (2014) and Ahern et al. (2016). In this study the impact of the laser vaporizer was not taken into consideration when calculating the CE because the amount of refractory material was rather low, and therefore, most of the chemical species were estimated to be

vaporized at the tungsten vaporizer. The uncertainty of the CE is discussed in supplemental material.

2.4.2. Positive matrix factorization

Sources of the particulate material were investigated by using Positive Matrix Factorization (PMF Tool 2.08D; Paatero and Tapper, 1994; Ulbrich et al., 2009). PMF was applied to the mass spectra of OA measured by the SP-AMS. PMF solutions were calculated up to eight factors (Fig. S3). It was found that a minimum of five factors were needed to explain the variation of OA in Valle Alegre. Based on their MS (Fig. S4a), these factors were identified as hydrocarbon-like OA (HOA), biomass burning OA (BBOA), semi-volatile oxygenated OA (SV-OOA), low-volatility oxygenated OA (LV-OOA) and marine oxygenated OA (MOOA). Compared to five factor solution, in four factor solution the typical fragments of BBOA and MOOA were mixed into the other factors whereas in the case of six, seven and eight factors HOA, LV-OOA and SV-OOA were split between several factors. PMF solutions with more than five factors did not give any additional information compared to five factor solution, and therefore, five factor solution was chosen to be presented and discussed in this article for OA (hereafter called OA-solution). Five factor solution was tested for the rotational freedom by varying fpeak, and also multiple seeds were calculated to confirm that the solution presented here was not a unique solution but could be achieved with various seeds.

In order to examine the sources of sulfate in Valle Alegre, PMF was also employed to the combined OA and sulfate MS (hereafter called OA + sulfate -solution). Sulfate fragments included in PMF were SO^+ (at m/z 48), HSO^+ (at m/z 49), SO_2^+ (at m/z 64), HSO_2^+ (at m/z 65), $H_2SO_2^+$ (at m/z 66), SO_3^+ (at m/z 80), HSO_3^+ (at m/z 81), $H_2SO_3^+$ (at m/z 82) and $H_2SO_4^+$ (at m/z 98). For both OA and sulfate, CE and RIE of 1 were used. Errors for the sulfate fragments were calculated similar to the fragments of OA. CO_2 and sulfate fragments were downweighed. This approach has also been used in e.g. Kortelainen et al. (2017), Tiitta et al. (2016) and Hao et al. (2014), but instead of sulfate, they included nitrate fragments in the matrix of OA. Due to the small concentration and contribution to mass (~2% of mass), nitrate was not included in PMF in this study. In addition to selected inorganic species, also a full mass spectrum encompassing all organic and inorganic components has been analyzed with PMF but that was performed in UMR mode (McGuire et al., 2014).

Similar to the PMF solution for OA, five factors, HOA, BBOA, SV-OOA, LV-OOA and MOOA, were obtained for OA + sulfate –solution (Fig. S4b). However, in OA + sulfate -solution there was an additional factor, called here as Sulfate factor, that consisted mostly of sulfate. Sulfate fragments were also found in MOOA and in smaller amount in LV-OOA and SV-OOA but in HOA and BBOA the amount of sulfate was very small.

PMF solutions for OA and OA + sulfate are compared for the MS in Fig. S4c and for the time series in Fig. S5a-b. Only organic fragments were included in the comparison. For HOA and BBOA, the MS and time series correlated well (R^2 = 0.939–0.999) except that for BBOA the fragments CO^+ (at m/z 28) and CO_2^+ (at m/z 44) were clearly smaller in the OA + sulfate -solution than in the OA-solution. Accordingly, for HOA the elemental composition of OA was very similar in the OA and OA + sulfate -solutions whereas for BBOA the oxygen to carbon ratio (O:C) was larger and the hydrogen to carbon ratio (H:C) smaller in the OA-solution than in the OA + sulfate -solution. For LV-OOA, the correlation between the time series of the OA and OA + sulfate -solutions was fairly good (R^2 = 0.966), however, most of the time LV-OOA concentrations were larger in the OA-solution than in the OA + sulfate -solution. The oxidation state was clearly lower in the OA-solution than in the OA + sulfate –solution for LV-OOA. For MOOA, the concentrations and oxidation states were rather similar for the OA and OA + sulfate –solutions. SV-OOA had the greatest difference between the OA and OA + sulfate -solutions. The correlation between the time series of the OA and OA + sulfate -solutions was only modest (R^2 = 0.725). Regarding the MS, the contributions of two main fragments, CO^+ and CO_2^+, were much larger, and accordingly SV-OOA was more oxidized, in the OA + sulfate –solution than in the OA-solution.

In terms of mass fractions (Fig. S5c), BBOA was equal in the OA- and OA + sulfate -solutions whereas SV-OOA was larger and HOA, LV-OOA and MOOA were smaller in the OA + sulfate than in the OA-solution. The additional sixth factor (Sulfate) contributed 9% to total OA in the OA + sulfate -solution. Sulfate factor had most similar O:C and H:C to BBOA. The PMF solution for OA + sulfate is utilized in this article only to evaluate the sources of sulfate in Valle Alegre (Section 3.3.2.). The discussion on the sources of OA (Section 3.3.1.) is based on the OA-solution.

3. Results and discussion

3.1. Meteorological parameters, air quality monitoring data and air mass origin

Daily-averaged meteorological conditions were rather stable during the measurement campaign in Valle Alegre. However, there was a clear diurnal cycle for wind speed and direction (Fig. 1c) dominated by the topography of the area as the measurement site was located in the valley (Fig. 1a). At night-time and morning, the dominant wind direction was northeast, typically from the bottom of the valley, and wind speed was low (< 0.5 m/s). Wind direction turned to south-west (the sea) around midday and also wind speed increased at the same time (hourly average maximum ~1.5 m/s). Temperature was on average (± stdev) 16.9 (± 1.7) °C during the campaign being around 3 °C higher in daytime than during night and early morning.

For the inorganic gases, the average (± stdev) concentrations were 2.6 (± 3.3), 4.5 (± 3.8), 20 (± 9.3) and 5.4 (± 6.1) ppb for NO, NO_2, O_3 and SO_2, respectively. The campaign-average (± stdev) PM_{10} concentration was 40 (± 16) μg m^{-3}. Of those species, only ozone displayed a clear diurnal trend (Fig. S6b). The concentration of ozone followed similar pattern to wind direction and speed increasing in the morning around 9 a.m. and having the maximum between 4 and 7 p.m. However, different from wind speed, ozone concentration remained at the elevated level later in the night while wind speed dropped at nighttime approximately at 10 p.m.

According to the backward trajectories, air masses arrived in Valle Alegre mostly from south or south-west (Fig. S7). Three days before arriving in Valle Alegre, air masses were over the Pacific Ocean and from there they travelled to Valle Alegre by following loosely the Chilean coastline from south to north. Occasionally air masses also made a loop over the continental Chile before reaching Valle Alegre. That happened mostly during the night and early morning. For example on 20 January 2015, air masses arrived in Valle Alegre from south-east from midnight to 9 a.m (Fig. S7c). after which the air mass trajectories turned to the sea. In general, the origin of air masses was rather similar during the whole measurement period. Small differences observed in the backward trajectories were not seen in the results, probably because the concentrations of air pollutants were mostly governed by local meteorology. Therefore, the trajectories are not discussed in this paper in the following sections.

3.2. Chemical composition of submicron particles

The campaign-average (± stdev) concentrations of organics, sulfate, nitrate, ammonium, chloride and BC were 4.9 (± 3.9), 3.3 (± 2.5), 0.14 (± 0.22), 0.99 (± 0.50), 0.06 (± 0.06) and 0.34 (± 0.35) μg m^{-3}, respectively, measured by the SP-AMS and MAAP (10-min averages). The concentrations of chemical species varied noticeably during the campaign. For organics and nitrate, the concentration peaks were rather short in time, typically from an hour to few hours, whereas for sulfate and ammonium, the concentrations varied in a longer time-scale, from several hours to almost a day (Fig. 2a). This

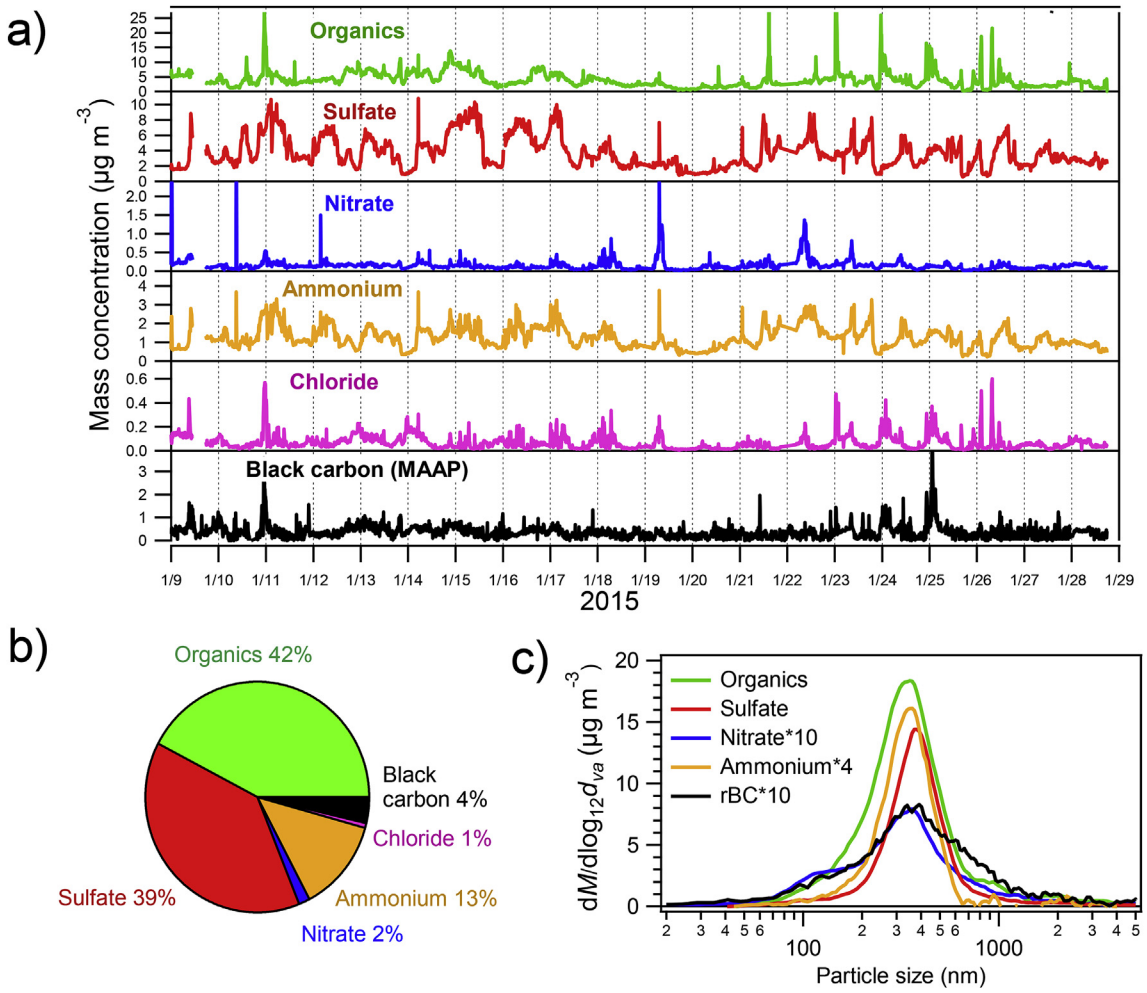

Fig. 2. The 10-min average concentrations of organics, sulfate, nitrate, ammonium, chloride and black carbon (a), the average composition of submicron mass (b) and mass size distributions (c). Chemical species were measured with the SP-AMS except BC that was taken from the MAAP in (a–b). In (c) the average mass size-distributions were calculated only for the period when the laser was on (9–18 January 2015) and m/z 36 was used as a surrogate for rBC. Note that in (c) nitrate and rBC concentrations were multiplied by a factor of 10 and ammonium by a factor of 4 in order to get them to the same scale.

suggested that sulfate and ammonium were mostly regionally dispersed whereas organics and nitrate originated also from the local sources such as vehicles or small-scale combustion. For BC, the concentration was rather stable throughout the campaign but there were some periods when BC was elevated. Regarding the total mass concentration of submicron particles, calculated by summing up all the species from the SP-AMS and MAAP, the campaign average concentration was 9.5 μg m^{-3}. Organics and sulfate had roughly similar mass fractions (42 and 39% on average, respectively) whereas the campaign-average contributions of ammonium, BC, nitrate and chloride to total mass were 13, 3.6, 1.6 and 0.7%, respectively (Fig. 2b and Fig. S8a).

The submicron mass concentration was smaller in Valle Alegre (9.5 μg m^{-3}) than that measured in rural (~13–20 μg m^{-3}) or urban (~20–50 μg m^{-3}) locations in Santiago Metropolitan Region (Carbone et al., 2013; Tagle et al., 2018). The most notable difference between Valle Alegre and Santiago was, however, the composition of submicron particles. In Valle Alegre, the mass fraction of sulfate (39%) was much larger than that in Santiago (< 10%) whereas the fraction of organics was larger in Santiago (~55% in Santiago). The small fraction of sulfate in Santiago can be explained by the lack of industrial sites and ports in Santiago area that were abundant in proximity to Valle Alegre. A large fraction of sulfate in submicron particles has been detected earlier e.g. at the urban sites in Pittsburgh, New York and Houston, USA (Zhang et al., 2007). By contrast, the mass fraction of nitrate was much larger in Santiago (~8–30%) than in Valle Alegre (~2%) due to the larger amount of traffic in Santiago. In general, the mass concentration of submicron particles in Valle Alegre was at the same level with the mass concentrations measured typically in urban areas but larger than the concentrations measured at rural locations (Zhang et al., 2007; Crippa et al., 2014).

Regarding the diurnal variations, none of the measured chemical species had a distinctive diurnal trend (Fig. S9). The clearest diurnal pattern was observed for chloride that had smaller concentrations at daytime from ~10 a.m. to 9 p.m. than in the other time of the day. Also the concentrations of organics and BC were slightly larger at night-time than daytime, however, the variation in concentrations was also greater during the night shown by the large standard deviations. Sulfate and ammonium concentrations followed loosely wind pattern (Fig. 1) being larger from midnight to midday when wind was from the valley and its speed was low resulting in the accumulation of pollutants in the boundary layer. After midday, the concentrations decreased as wind started to blow from the sea and the mixing of atmospheric species increased. For nitrate, there was a peak in concentrations between 7 and 9 a.m. that could be due to morning traffic, however, at that time of the day nitrate concentrations varied a lot shown by the large standard deviations.

In terms of mass size distributions, most of the chemical species had an accumulation mode with a maximum at ~350 nm (Fig. 2c). Ammonium peaked at slightly smaller particle size than sulfate. The size distributions of organics and nitrate deviated from those of ammonium

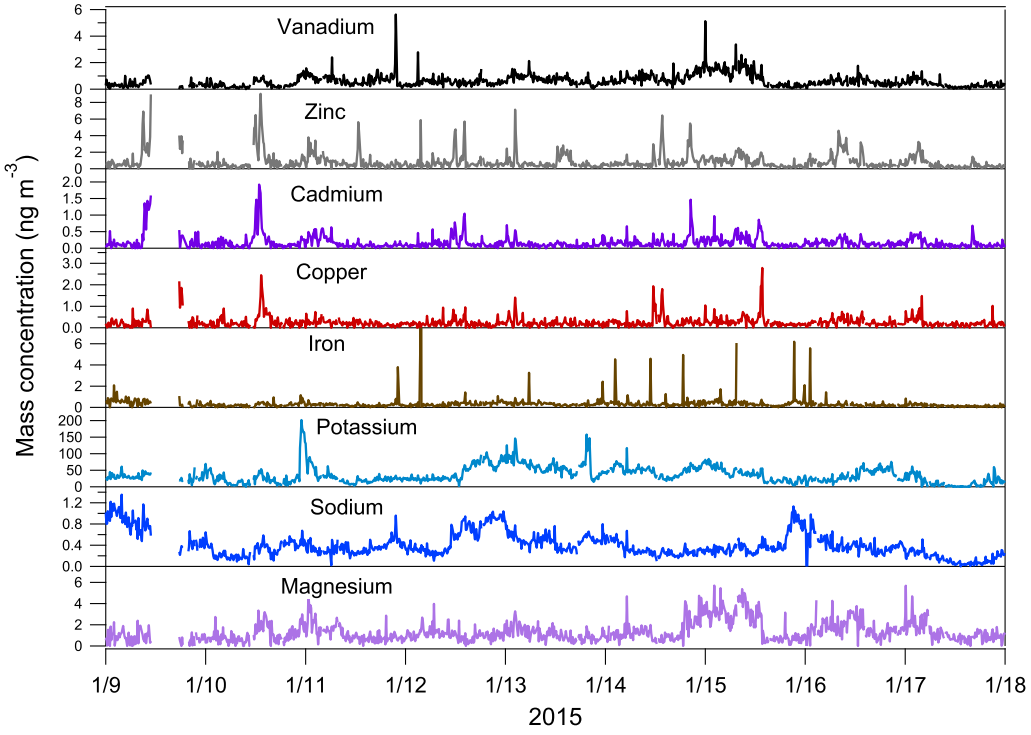

Fig. 3. Time series of metals detected in submicron particles using the SP-AMS; 10-min average concentrations for the period when the laser was on.

and sulfate. Organics had slightly wider accumulation mode than ammonium and sulfate having relatively more mass at < 350 nm whereas nitrate had an additional mode at ~100 nm. The time evolution of the size distributions (Fig. S10) revealed that organics and nitrate were found in small particles only in short time periods that is in agreement with the earlier speculation that nitrate and organics originated also from local sources, probably from traffic or small-scale burning. For BC, the mass size distribution was calculated by using unit mass resolution m/z 36 (that consists mostly of C_3^+ fragment) as a surrogate for rBC in the SP-AMS. The mass size distribution of rBC was similar to that of nitrate except that the accumulation mode extended to larger particle sizes for rBC. That indicates that a larger contribution of rBC was transported to site from distant sources supported by a more steady concentration of rBC compared to that of nitrate.

3.2.1. Organics

The average mass spectrum for organics is shown in Fig. S11. The dominant organic fragments were CO^+ (at m/z 28) and CO_2^+ (at m/z 44) fragments indicating that organics were highly oxidized. In general, oxygenated fragments ($C_xH_yO_z^+$) constituted 54% of organics of which slightly more than half contained the fragments with one oxygen atom (e.g. CO^+) whereas the other portion included the fragments with more than one oxygen atom (mostly CO_2^+). The rest of organics consisted of hydrocarbon fragments ($C_xH_y^+$) that had largest signal for CH_3^+ (at m/z 15), $C_2H_3^+$ (at m/z 27), $C_3H_3^+$ (at m/z 39) and $C_3H_5^+$ (at m/z 41). Regarding the elemental composition of organics, the average (± stdev) H:C and O:C were 1.5 (± 0.14) and 0.68 (± 0.19), respectively, resulting in the average (± stdev) ratio of 2.0 (± 0.25) for the organic matter to organic carbon ratio (OM:OC). O:C and OM:OC were slightly larger from 3 p.m. to around 9 p.m., and H:C accordingly smaller, than at the other times of the day (Fig. S12). The larger O:C and OM:OC in the afternoon indicated the formation of secondary organic aerosol (SOA) because also the concentration of oxidants (sum of O_3 and NO_2; Fig, S6b) was clearly larger in the afternoon. However, since also wind direction changed around midday, it is difficult to distinguish unambiguously the impact of oxidation from different source areas. The sources and oxidation states of different OA fractions are discussed later with the PMF results (Section 3.3.1.).

A small fraction (~1%) of organic fragments contained also sulfur atoms ($C_xH_yO_zS^+$). The largest sulfur-containing fragments were CH_2SO^+ (at m/z 62), CH_3SO^+ (at m/z 63), $CH_2SO_2^+$ (at m/z 78) and $CH_3SO_2^+$ (at m/z 79). The concentrations of CH_2SO^+, $CH_2SO_2^+$ and $CH_3SO_2^+$ depended slightly on the time of the day (Fig. S13). They all had a minimum around midday while $CH_2SO_2^+$ and $CH_3SO_2^+$ had also a clear maximum between 6 and 8 p.m. Sulfur to carbon ratio (S:C) for organics was on average (± stdev) 2.3 (± 1.6)*10^{-3}.

Detected sulfur-containing fragments are typical fragments of MSA that is an oxidation product of dimethyl sulfide (DMS) produced by marine phytoplankton in the marine atmosphere (Charlson et al., 1987; Schmale et al., 2013). In addition to the $C_xH_yO_zS^+$ fragments, MSA produces sulfur-containing organic fragments without oxygen atoms; CHS^+ (at m/z 45) and CH_3S^+ (at m/z 47). Those fragments were also found in Valle Alegre but their concentrations were more uncertain as they were overlapped by large organic fragments at the same nominal m/z's (CHO_2^+ at m/z 45 and $CH_3O_2^+$ at m/z 47). MSA-related organic fragments will be investigated in more detail in Section 3.3.1.

In addition to MSA, sulfur-containing fragments (specifically $CH_3SO_2^+$) can also originate from the fragmentation of organosulfates (i.e., $ROSO_3H$; Farmer et al., 2010; Huang et al., 2015). In the AMS mass spectra, organosulfates are detected as separate organic and sulfate fragments, however, pure organosulfur fragments are found only in minor amounts. Regarding inorganic fragments, the fragmentation of organosulfates is similar to that of inorganic sulfate (Farmer et al., 2010). Organosulfates can be produced e.g. from the oxidation of biogenic precursors in the presence of sulfate aerosol (Surratt et al., 2008). Besides sulfur-containing organic fragments, a minor fraction (~1%) of organic fragments contained nitrogen atoms ($C_xH_yN^+$) the signal being clearest for CH_4N^+ (at m/z 30). The average (± stdev) nitrogen to carbon ratio (N:C) was 7.0 (± 9.5)*10^{-3}.

3.2.2. Metals and inorganic salts

V, Zn, Fe, Cd, Cu, K, Na and Mg were detected in the particles in Valle Alegre. The concentrations of metals were calculated for the period when the laser vaporizer was on (9–18 January 2015). The

general assumption was that the metals were vaporized only with the laser, however, some metals (Zn, Cu, Na, K and Mg) were also observed during the period when the laser was off. Those metals were probably associated with some inorganics salts and/or vaporized with the tungsten vaporizer (Salcedo et al., 2012).

The average (± stdev) concentrations for V, Zn, Fe, Cd, Cu, K, Na and Mg were 0.65 (± 0.80), 1.6 (± 2.3), 0.48 (± 2.3), 0.10 (± 0.15), 0.53 (± 0.76), 70 (± 103), 22 (± 20) and 2.6 (± 2.2) ng m^{-3}, respectively. Regarding the time evolution of metals, Fe had very short-lived concentration peaks whereas the concentrations of other metals changed more slowly (Fig. 3). Zn, Cd and Cu had some similarities in their time series but clear correlations between metals were not found. The largest concentration peak for Zn, Cd and Cu was observed on 10 January 2015 from midday to ~2 p.m. During that time also organics and sulfate concentration increased, but not ammonium (Fig. 2a), indicating that aerosol was acidic. Also gas phase NO and SO_2 concentrations were slightly elevated (Fig. S6a). It can be speculated that the increase in metal concentrations during that period can be due to the emissions from the industrial sites, however, that could not be verified since wind direction was between west and south-west while industrial sites were located north-west from the measurement site.

Diurnal variation was observed only for V and Mg (Fig. S14). They had slightly smaller concentrations in the afternoon, similar to sulfate (Fig. S9). Accordingly, the concentration of Mg somewhat correlated with that of sulfate (R^2 = 0.45). Mg and Ca were found as chloride salts ($MgCl_2^+$ at m/z 94 and $CaCl_2^+$ at m/z 110) but it was not possible to determine Ca itself due to the overlapping argon peak at m/z 40. $MgCl_2^+$ and $CaCl_2^+$ followed the time trend of Cd (Fig. S15) suggesting that their origin could be sea water as also Cd is found in sea water (Boyle et al., 1976). However, the time series of Na, chloride and $NaCl^+$ (at m/z 58) were different from that of $MgCl_2^+$, $CaCl_2^+$ and Cd (Fig. S15) indicating that the source was probably other than sea-water.

K had a large concentration peak on 10–11 January 2015 from 10:30 p.m. to around 1 a.m. (Fig. 3). At the same time also PM_{10} (Fig. S6a), organics and BC (Fig. 2a), and KCl^+ (at m/z 74; Fig. S15) had elevated concentrations. KCl^+ followed more closely the time trend of chloride than that of K. Elevated concentration on 10 January were likely to be caused by biomass burning. PMF analysis in Section 3.3.1 confirms that organics originated from biomass burning at that time. In general, K had rather similar time series with organics and BC (R^2 = 0.58 and R^2 = 0.44, respectively) indicating that a part of organics and BC may originate from biomass burning. The influence of biomass burning on the concentration of organics will be shown in Section 3.3.1.

K was also detected as KNO_3^+ fragment (at m/z 101). In some cases, KNO_3^+ concentration increased together with nitrate (Fig. S15), however, there was no correlation when calculated over the whole data set. KNO_3^+ can be speculated to be related to fertilizers used in agriculture as the site was located in agricultural area. KNO_3^+ can also originate from biomass burning because KCl, a species that is found in fresh biomass burning smoke, can react with nitrate and form KNO_3.

3.3. Source apportionment

3.3.1. Source apportionment for organic aerosol

The sources and atmospheric processing of OA in Valle Alegre were investigated by using PMF. PMF for OA resolved five factors; HOA, BBOA, SV-OOA, LV-OOA and MOOA. High resolution mass spectra, time series and diurnal trends for the factors are shown in Fig. 4. On average, oxygenated secondary OA factors (LV-OOA, SV-OOA and MOOA) constituted 75% of total OA. LV-OOA had the largest contribution to OA individually (38%) followed by MOOA (21%) and SV-OAA (16%; Fig. S5c). Regarding primary OA, the contribution of HOA was larger (15%) than that of BBOA (10%).

The MS of HOA was dominated by hydrocarbon fragments ($C_xH_y^+$) of which the largest signal found for $C_3H_5^+$ (at m/z 41), $C_4H_7^+$ (at m/z 55) and $C_3H_7^+$ (at m/z 43). The MS of HOA resembled to the standard MS profile given in Ng et al. (2011; R^2 = 0.917) but it was even more similar to the MS measured previously in Mexico City (Aiken et al., 2009; R^2 = 0.965), Helsinki (Carbone et al., 2014; R_2 = 0.946) and Xi'an and Beijing (Elser et al., 2016; R^2 = 0.931) (Fig. S16). HOA is typically associated with traffic emissions (Zhang et al., 2005). In terms of vehicle emissions, the MS of HOA in Valle Alegre was more similar to that of a gasoline vehicle (Timonen et al., 2017) than that of a diesel bus (Saarikoski et al., 2017). This finding is in agreement with the vehicle fleet in Chile that consist mostly (~80%) of gasoline cars. HOA was very lightly oxygenated having high H:C (1.95) and very low O:C (0.09). Compared to the previous studies, HOA was less oxidized in Valle Alegre than e.g. in Po Valley (O:C 0.20; Saarikoski et al., 2012) or Mexico City (O:C 0.16; Aiken et al., 2009) but close to that measured in the Pearl River Delta region in China (O:C 0.11; He et al., 2011). In general, the concentration of HOA was rather small most of the time but there were some periods, typically from an hour to few hours, when HOA concentration increased and HOA dominated OA (Fig. 4b and S8b). Regarding the diurnal variation, HOA displayed slightly larger concentrations during the night than at daytime, however, also the variation in HOA concentrations was large during the night. Even though HOA time trend somewhat followed to that of BC, HOA did not correlate with BC, or nitrogen oxides (NO, NO_2, NO_x) suggesting that there could be some additional sources for HOA besides vehicles.

The MS of BBOA had a large signal for CHO^+ (at m/z 29) and $C_2H_3^+$ (at m/z 27) but also the oxygenated fragments $C_2H_4O_2^+$ (at m/z 60) and $C_3H_5O_2^+$ (at m/z 73), that have been earlier associated with biomass burning (Alfarra et al., 2007), were elevated. Oxygenated fragments $C_2H_4O_2^+$ and $C_3H_5O_2^+$ contributed 2.9 and 1.2%, to the total signal of BBOA, respectively. BBOA was clearly more oxidized than HOA having larger O:C (0.36) and smaller H:C (1.78) than HOA. BBOA was more oxidized in Valle Alegre than in Po Valley (O:C 0.23; Saarikoski et al., 2012), Mexico City (O:C 0.30; Aiken et al., 2009) or the Pearl River Delta region (O:C 0.32; He et al., 2011). Regarding the time series, BBOA concentration was elevated during four periods. The largest BBOA concentration was measured on 23 January after midnight but BBOA was also elevated on 10–11 January at the same time with K as discussed earlier in Section 3.2.2. In general, BBOA and K had some similarities in their time trends with the correlation coefficient R^2 = 0.47. BBOA correlated more clearly with BC than HOA (R^2 = 0.47) suggesting that the observed BC concentrations were probably partly associated with biomass combustion. BBOA had also a moderate correlation with chloride (R^2 = 0.43). In terms of diurnal variation BBOA had elevated concentrations at night-time, with a large variation in concentrations, similar to HOA.

SV-OOA had most pronounced signal for $C_2H_3O^+$ (at m/z 43) followed by $C_2H_3^+$ (at m/z 27), $C_3H_3^+$ (at m/z 39) and $C_3H_5^+$ (at m/z 41). SV-OOA was slightly more oxygenated than BBOA with O:C and H:C ratios of 0.37 and 1.62, respectively. Regarding the diurnal trend, SV-OOA was slightly elevated in the morning (maximum at ~8–12 a.m.) after which it decrease towards the evening having minimum at ~7–10 p.m. The diurnal trend of SV-OOA somewhat agreed to that of nitrate (Fig. S9), however, nitrate concentration was elevated much shorter time period than SV-OOA concentration. Different from the time series of HOA and BBOA that had several short-term peaks, SV-OOA concentration was steadier throughout the campaign. SV-OOA had only one short-term maximum on 23 January after midnight together with BBOA. On 23 January SV-OOA seemed to be related to biomass burning. Previously, it has been suggested that biomass burning can produce OOA-type aerosol indicated by a stronger correlation between levoglucosan (marker compound for biomass burning) and OOA components than levoglucosan and BBOA (Saarikoski et al., 2012).

The largest fraction (38%) of OA consisted of LV-OOA. LV-OOA was clearly the most oxygenated factor having O:C and H:C of 1.19 and 1.22, respectively, and its MS dominated by CO_2^+ (at m/z 44) and CO^+ (m/z 28) fragments. LV-OOA had very flat diurnal trend with no

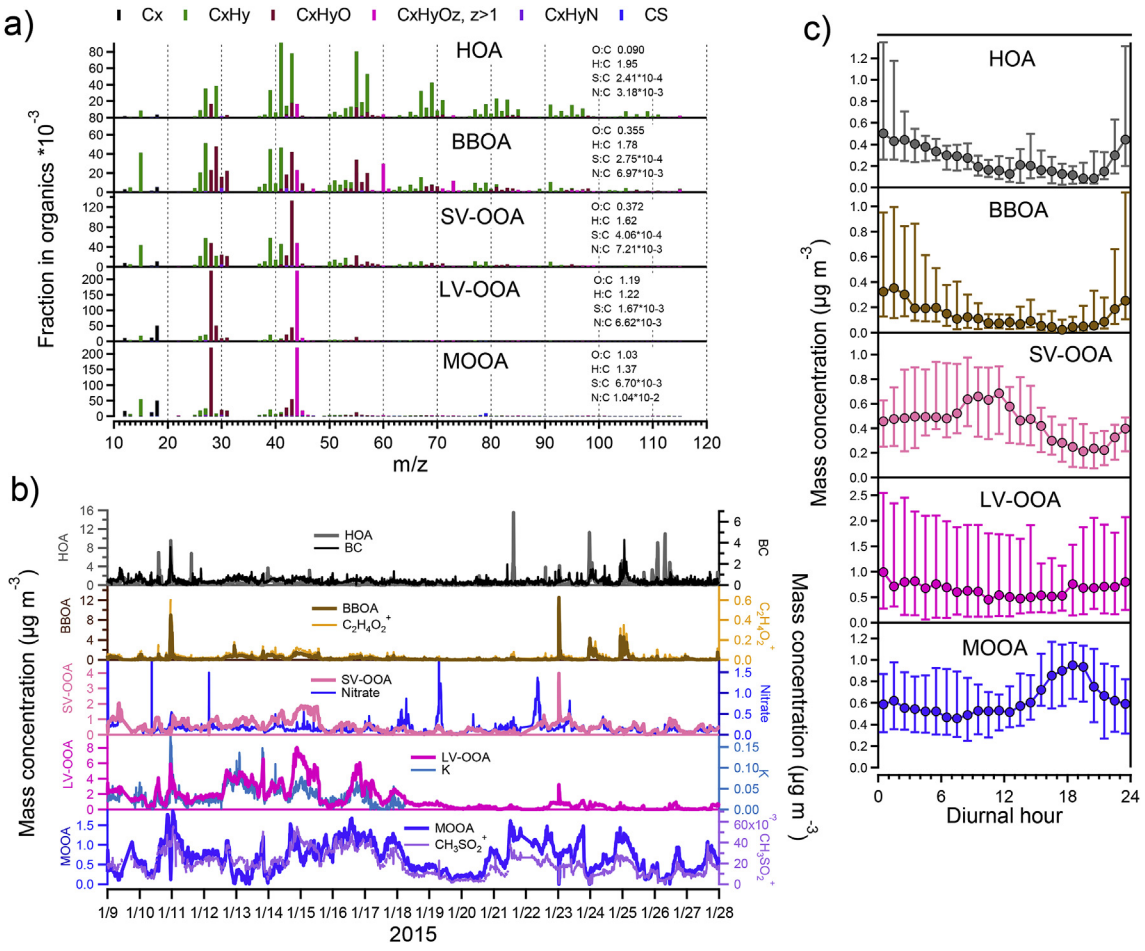

Fig. 4. PMF factors for organic aerosol. Mass spectra (a), time series with tracers (a) and diurnal trends (median ± 25/75%) (c). CS species in (a) refer both to $C_xH_yO_zS^+$ and $C_xH_yS^+$ fragments.

dependence on the time of the day but the LV-OOA concentrations were clearly larger at the beginning of the campaign than at the end. Also LV-OOA seemed to be somewhat associated with biomass burning as LV-OOA correlated stronger with K than BBOA (R^2 = 0.51). By looking at the time series of K, it was noticed that the largest K peaks were captured by BBOA whereas the general time-evolution of K was followed more closely by LV-OOA. As already mentioned, OOA can originate from biomass burning, however, it is also possible that the correlation of LV-OOA and K was related to the transport of regional/long-range transported pollutants.

On average, MOOA made 21% of total OA. In terms of diurnal variation, MOOA was clearly larger in the evening, which suggested it to be marine-related as wind blew from sea at that time of the day (Fig. S17). The maximum of MOOA (at ~7 p.m.) was probably related to the SOA formation peaking at the early evening as did also the oxidants ($O_3 + NO_2$; Fig, S6b). The MS of MOOA was similar to that of LV-OOA having the largest signal for CO_2^+ (at m/z 44) and CO^+ (at m/z 28) and displaying the second largest O:C ratio (1.03) after LV-OOA. MOOA had a clear signal for the fragments $CH_2SO_2^+$ (at m/z 78) and $CH_3SO_2^+$ (at m/z 79) with their fractions in MOOA being 0.32 and 0.94%, respectively. Also CH_2SO^+ (at m/z 62) and CH_3SO^+ (at m/z 63) were present in the MS of MOOA but with smaller amounts (< 0.2%). As already mentioned these fragments are typical for MSA that is primarily derived from the oxidation of DMS in marine environment, and therefore, can be considered as a tracer for marine SOA. Also sulfur-containing organic fragments without oxygen atoms CHS^+ (at m/z 45) and CH_3S^+ (at m/z 47) were associated with MOOA having the contributions of 0.26 and 0.05%, respectively.

Sulfur-containing organic fragments found in MOOA were compared to the reference MS of MSA obtained in the laboratory tests (Fig. S18). The pattern of CH_2SO^+ (at m/z 62), CH_3SO^+ (at m/z 63), $CH_2SO_2^+$ (at m/z 78) and $CH_3SO_2^+$ (at m/z 79) was very similar to MOOA and MSA standard whereas the relative contributions of CHS^+ (at m/z 45) and $CH_4SO_3^+$ (at m/z 96) were larger for MSA than for MOOA. One reason for the difference can be that CHS^+ and $CH_4SO_3^+$ are difficult to separate from overlapping peaks at same m/z when they are present in small quantities (in MOOA). Based on the ratio of $CH_3SO_2^+$ to the total organic signal in the reference MS of MSA (0.11), the contribution of MSA to MOOA was estimated to be 8.5%.

Due to the presence of sulfur-containing fragments in MOOA, S:C was several times larger for MOOA ($6.7*10^{-3}$) than that for the other PMF factors ($0.24–1.7*10^{-3}$). Also N:C was largest for MOOA ($1.0*10^{-2}$). That is in line with the previous finding that biogenic amines are an important source of marine secondary aerosol (Facchini et al., 2008). In addition to MOOA, nitrogen-containing fragments were observed in BBOA and SV-OOA.

3.3.2. Source apportionment for sulfate

The sources of sulfate in Valle Alegre were investigated by adding sulfate fragments to the data matrix analyzed with PMF. PMF for OA + sulfate resulted in six factors of which five factors were similar to those without the sulfate fragments whereas sixth factor was dominated by sulfate (called Sulfate factor). The comparison between OA and OA + sulfate factors was presented earlier in Section 2.4.2. (Experimental methods).

The distribution of sulfate between the PMF factors is shown in

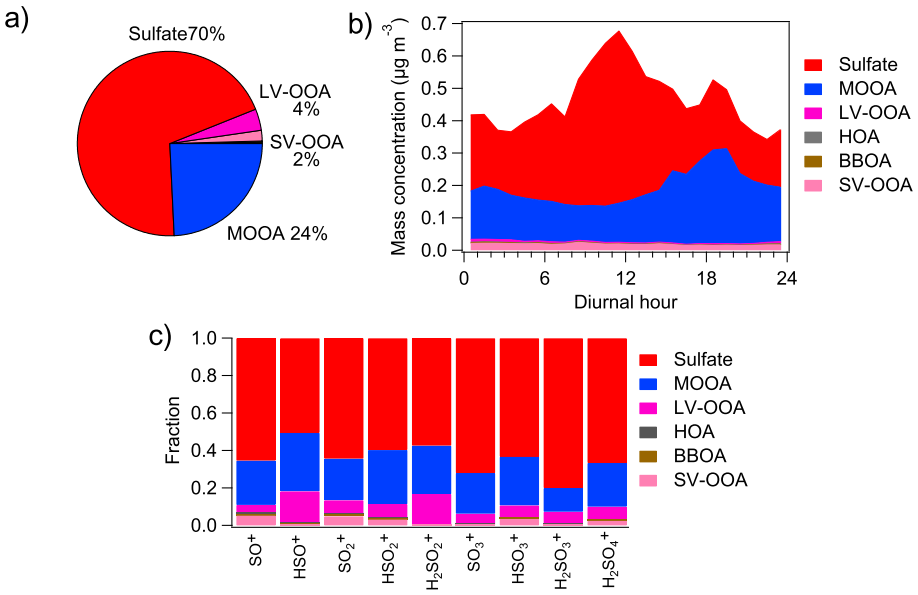

Fig. 5. Distribution of sulfate between the PMF factors in terms of total mass (a) diurnal hour (b), and individual fragments (c).

Fig. 5a. Sulfate have two major sources, or formation paths, in Valle Alegre. On average, 70% of sulfate was related to Sulfate factor that was assumed to be related to the oxidation of anthropogenic SO_2. The time evolution of Sulfate factor followed that of SO_2 at times (Fig. S19a) but there was no clear correlation between Sulfate factor and SO_2 in general. The lack of correlation between SO_2 and sulfate can be due to the fact that SO_2 is a primary component while sulfate is formed from the oxidation of SO_2. Therefore, their concentration ratio depends on the oxidation time of SO_2 as well as the removal efficiencies for both SO_2 and sulfate. Sulfate factor, however, somewhat correlated with the acidity of particles (Fig S19b).

The second largest fraction of sulfate was associated with marine-related OA (MOOA; 24%). Sulfate in MOOA was assumed to be related to the oxidation of DMS in the marine environment because, in addition to MSA, the oxidation of DMS produces SO_2 which is oxidized to sulfate in the atmosphere. A small portion of sulfate was also associated with LV-OOA and SV-OOA (4 and 2%, respectively) whereas HOA and BBOA contained only a negligible fraction of total sulfate (< 1%; not shown in Fig. 5a).

The origin of sulfate depended clearly on the time of the day (Fig. 5b). From midnight until ~4 p.m. the largest fraction of sulfate was attributed to Sulfate factor, its contribution being especially large between 6 a.m. and 4 p.m., whereas in the evening a greater portion of sulfate was associated with MOOA. The diurnal trend for sulfate in Sulfate factor followed that of SV-OOA (Fig. 4c) suggesting that they were both products of local secondary aerosol formation. In the Valle Alegre area, the major industrial sources of SO_2, the copper sulfate smelter and coal-fired power plants, are located ~12 km from the measurement site. The maximum for sulfate in MOOA in the evening coincided with the maximum concentration of oxidants (S6b).

Regarding different sulfate fragments, none of the fragments was clearly attributed to specific PMF factor. All the fragments were mostly related to the Sulfate-factor (Fig. 5c). Sulfate factor had the largest contribution to $H_2SO_3^+$ (85%) and smallest to HSO^+ (56%) whereas the opposite was detected to MOOA having the largest contribution to HSO^+ (31%) and smallest to $H_2SO_3^+$ (13%). HSO^+ and $H_2SO_2^+$ were also partly associated with LV-OOA (11%), and SO^+ and SO_2^+ were associated with SV-OOA (~4%).

Sulfate from the oxidation process of DMS is often called non-sea salt sulfate (nss-sulfate) in order to distinguish it from sulfate originated from sea-salt in the marine environment. Since the oxidation of DMS can be considered to be the only atmospheric source of MSA, MSA can be used as a tracer to separate marine biogenic sulfate from the other sulfate sources (Davis et al., 1999; Legrand et al., 1991). The ratio of MSA to nss-sulfate, however, depends on the ambient condition such as temperature (Bates et al., 1992). In this study, for MOOA, the ratio of MSA to nss-sulfate was 0.11 when MSA was calculated by using the ratio of $CH_3SO_2^+$ to the total organic signal in the reference MS of MSA and nss-sulfate was calculated by using the measured Na concentration (> 99% of total sulfate in MOOA was nss-sulfate). This ratio was in the same magnitude, or slightly larger, than that observed earlier in South Pacific (0.010–0.210), however, modelled MSA to nss-sulfate ratios were typically larger (0.093–0.205; Gondwe et al., 2004). The ratio of MSA to nss-sulfate obtained in this study suggested that most of sulfate in MOOA was likely to be associated with marine origin, DMS oxidation.

Besides sulfate from the oxidation of DMS, the fragmentation of MSA produces inorganic fragments similar to sulfate. Therefore, the pattern of sulfate fragments detected for MOOA and Sulfate factor was compared to the pattern observed for MSA and ammonium sulfate in the laboratory (Fig. S18). It is clear that the sulfate pattern for MOOA and Sulfate-factor resembled the pattern of ammonium sulfate more than that of MSA. MSA had relatively larger contribution of HSO_2^+ (at m/z 65) than ammonium sulfate, MOOA or Sulfate-factor whereas SO_3^+ (at m/z 80) was almost absent in the MS of MSA. It can be concluded that most of sulfate in MOOA and Sulfate-factor was related to inorganic sulfate (ammonium sulfate, ammonium bisulfate, sulfuric acid) not organic sulfur, like MSA. That was also confirmed by calculating the amount of sulfate formed from the fragmentation of MSA by using the ratio of total sulfate to $CH_3SO_2^+$ obtained from the reference MS of MSA (Fig. S18). Based on this calculation, ~17% of sulfate in MOOA (and 2.5% in Sulfate-factor) was attributed to the fragmentation of MSA. As already mentioned sulfur-containing organic and inorganic fragments may also originate from the fragmentation of organosulfates (Farmer et al., 2010) but their contribution could not be taken into account in this study.

4. Conclusions

The aim of this study was to investigate the chemical composition and sources of submicron particles in Valle Alegre, the coastal area of Central Chile. The specific feature of the measurement location was the vicinity of large natural particle source (Pacific Ocean) and several anthropogenic sources (industrial area). In general, Valle Alegre is

considered rather polluted as the mass concentrations often exceed the national air quality standards for PM_{10}, $PM_{2.5}$ and SO_2. However, the average mass concentration for submicron particles during the three-week campaign was only 9.5 μg m^{-3} that corresponds with the mass concentrations measured typically in urban areas (e.g. Zhang et al., 2007). The reason for the rather small concentration was likely to be the location of the measurement site that was in a corner of agricultural and recreational area not supposed to represent the most polluted location in the valley.

Particles were dominated by organic compounds (42% of mass). Organic aerosol were largely influenced by secondary OA that was mostly long-range transported, or regionally distributed highly-oxygenated material (LV-OOA), or marine-related (MOOA). The specific feature of MOOA was that, in addition to oxygenated organic fragments, it contained organic fragments with sulfur. Sulfur-containing fragments were associated with the fragmentation of MSA (CH_2SO^+, $CH_2SO_2^+$ and $CH_3SO_2^+$). Additionally, a factor probably representing local SOA production was detected (SV-OOA). A smaller fraction of OA was composed of primary OA (HOA and BBOA) that probably originated from local combustion sources, traffic and biomass burning. Direct industrial-related OA could not be identified in this study. However, based on the PMF solution for OA and sulfate, 9% of OA was attributed to the PMF factor related to anthropogenic sulfate. This is higher OA fraction than that found in a previous study conducted in an industrialized environment in Marseille, France, where ~5% of total OA was associated with industry (El Haddad et al., 2013).

Submicron particles contained a significant fraction of sulfate (39% of mass). Sulfate was partly neutralized by ammonium but there were periods when particles were clearly acidic. Sulfate had two major sources, or formation pathways, in Valle Alegre. 70% of sulfate seemed to be related to the oxidation of anthropogenic SO_2 whereas 24% of sulfate was associated with the oxidation of DMS in the marine environment. The most important industrial sources of sulfate at the area were copper smelter and coal-fired power plants. The concentrations of other inorganics species, nitrate, BC and chloride, were rather small peaking only in few cases, their sources being possibly quite local.

Due to the laser vaporizer, the SP-AMS also allowed to detect metals (V, Zn, Fe, Cd, Cu, K, Na and Mg) in submicron particles. The time series of Zn, Cd and Cu resembled each other suggesting same origin that was speculated to be industry as also sulfate and SO_2 concentration were elevated at the same time. However, separating the sources of particles was a challenge because the industrial sites and sea were located at the same direction from the measurement site. Some of the metals were also found as inorganic salts of chloride and nitrate ($NaCl^+$, $MgCl_2^+$, $CaCl_2^+$, KCl^+ and KNO_3^+) likely to be related to both natural and anthropogenic origin.

Overall, secondary species constituted 84% of total submicron particle mass in Valle Alegre when BBOA, HOA and BC were considered as primary components. Large contribution of secondary mass can be explained by high concentration of atmospheric oxidants, since the measurements were conducted in summertime, but also by several industrial sources in the region that emit sulfate precursor SO_2. The impact of anthropogenic and biogenic sources on total mass was somewhat equal when sulfate from anthropogenic SO_2 oxidation, BC, nitrate, ammonium, chloride and primary OA (HOA and BBOA) were assumed to be anthropogenic, and sulfate from DMS oxidation and all OOA fractions biogenic. However, if OOA originated also from anthropogenic sources, anthropogenic particle mass exceeded biogenic particle mass. Purely marine-related was ~19% of mass (MOOA and sulfate from DMS oxidation) and ~18% of mass was from combustion sources (HOA, BBOA and BC).

This study showed that the contribution of anthropogenic and biogenic (marine) sources to organic and inorganic particulate matter can be identified and separated. The results of this study provided valuable, novel information on the characteristics and sources of submicron particles in the rural location influenced by industrial and marine sources especially abundant of sulfur-containing inorganic and organic species. Although the measurements were carried out in a single location for a rather short time, the results and the applied measurement and data analysis methods are also applicable to other similar areas to some extent. To our knowledge this is the most extensive study characterizing the chemical properties of submicron particles in coastal Chile.

Acknowledgements

This work was funded by the Academy of Finland (grant no 259016 and project no 297804; PARMAT), Tekes (HIME-project) and the Ministry of Environment, Chile.

Appendix A. Supplementary data

Supplementary data to this article can be found online at https://doi.org/10.1016/j.atmosenv.2018.11.040.

References

Ahern, A.T., Subramanian, R., Saliba, G., Lipsky, E.M., Donahue, N.M., Sullivan, R.C., 2016. Effect of secondary organic aerosol coating thickness on the real-time detection and characterization of biomass-burning soot by two particle mass spectrometers. Atmos. Meas. Tech. 9, 6117–6137.

Aiken, A.C., DeCarlo, P.F., Jimenez, J.L., 2007. Elemental analysis of organic species with electron ionization high resolution mass spectrometry. Anal. Chem. 79, 8350–8358. https://doi.org/10.1021/ac071150w.

Aiken, A.C., DeCarlo, P.F., Kroll, J.H., Worsnop, D.R., Huffman, J.A., Docherty, K., Ulbrich, I.M., Mohr, C., Kimmel, J.R., Sueper, D., Sun, Y., Zhang, Q., Trimborn, A., Northway, M., Ziemann, P.J., Canagaratna, M.R., Onasch, T.B., Alfarra, M.R., Prevot, A.S.H., Dommen, J., Duplissy, J., Metzger, A., Baltensperger, U., Jiménez, J.L., 2008. O/C and OM/OC ratios of primary, secondary, and ambient organic aerosols with a high resolution time-of-flight aerosol mass spectrometer. Environ. Sci. Technol. 42, 4478–4485.

Aiken, A.C., Salcedo, D., Cubison, M.J., Huffman, J.A., DeCarlo, P.F., Ulbrich, I.M., Docherty, K.S., Sueper, D., Kimmel, J.R., Worsnop, D.R., Trimborn, A., Northway, M., Stone, E.A., Schauer, J.J., Volkamer, R.M., Fortner, E., de Foy, B., Wang, J., Laskin, A., Shutthanandan, V., Zheng, J., Zhang, R., Gaffney, J., Marley, N.A., Paredes-Miranda, G., Arnott, W.P., Molina, L.T., Sosa, G., Jimenez, J.L., 2009. Mexico City aerosol analysis during MILAGRO using high resolution aerosol mass spectrometry at the urban supersite (T0) – Part 1: fine particle composition and organic source apportionment. Atmos. Chem. Phys. 9, 6633–6653.

Alfarra, M.R., Prevot, A.S.H., Szidat, S., Sandradewi, J., Weimer, S., Lanz, V.A., Schreiber, D., Mohr, M., Baltensperger, U., 2007. Identification of the mass spectral signature of organic aerosols from wood burning emissions. Environ. Sci. Technol. 41, 5770–5777.

Bates, T.S., Calhoun, J.A., Quinn, P.K., 1992. Variations in the methanesulfonate to sulfate molar ratio in submicrometer marine aerosol particles over the South Pacific Ocean. J. Geophys. Res. 97, 9859–9865.

Boyle, E.A., Sclater, F., Edmond, J.M., 1976. On the marine geochemistry of cadmium. Nature 263, 42–44.

Canagaratna, M.R., Jimenez, J.L., Kroll, J.H., Chen, Q., Kessler, S.H., Massoli, P., Hildebrandt Ruiz, L., Fortner, E., Williams, L.R., Wilson, K.R., Surratt, J.D., Donahue, N.M., Jayne, J.T., Worsnop, D.R., 2015. Elemental ratio measurements of organic compounds using aerosol mass spectrometry: characterization, improved calibration, and implications. Atmos. Chem. Phys. 15, 253–272.

Carbone, S., Aurela, M., Saarnio, K., Saarikoski, S., Frey, A., Timonen, H., Sueper, D., Ulbrich, I., Jimenez, J.-L., Kulmala, M., Worsnop, D., Hillamo, R., 2014. Wintertime aerosol chemistry in sub-arctic urban air. Aerosol Sci. Technol. 48, 312–322.

Carbone, S., Onasch, T., Saarikoski, S., Timonen, H., Saarnio, K., Sueper, D., Rönkkö, T., Pirjola, L., Worsnop, D., Hillamo, R., 2015. Characterization of trace metals with the SP-AMS: detection and quantification. Atmos. Meas. Tech. 8, 4803–4815.

Carbone, S., Saarikoski, S., Frey, A., Reyes, F., Reyes, P., Castillo, M., Gramsch, E., Oyola, P., Jayne, J., Worsnop, D.R., Hillamo, R., 2013. Chemical characterization of submicron aerosol particles in Santiago de Chile. Aerosol Air Qual. Res. 13, 462–473.

Charlson, R.J., Lovelock, J.E., Andreae, M.O., Warren, S.G., 1987. Oceanic phytoplankton, atmospheric sulphur, cloud albedo and climate. Nature 326, 655–661.

Crippa, M., Canonaco, F., Lanz, V.A., Äijälä, M., Allan, J.D., Carbone, S., Capes, G., Dall'Osto, M., Day, D.A., DeCarlo, P.F., Di Marco, C.F., Ehn, M., Eriksson, A., Freney, E., Hildebrandt Ruiz, L., Hillamo, R., Jimenez, J.-L., Junninen, H., Kiendler-Scharr, A., Kortelainen, A.-M., Kulmala, M., Mensah, A.A., Mohr, C., Nemitz, E., O'Dowd, C., Ovadnevaite, J., Pandis, S.N., Petäjä, T., Poulain, L., Saarikoski, S., Sellegri, K., Swietlicki, E., Tiitta, P., Worsnop, D.R., Baltensperger, U., Prévôt, A.S., 2014. Organic aerosol components derived from 25 AMS datasets across Europe using a newly developed ME-2 based source apportionment strategy. Atmos. Chem. Phys. 14, 6159–6176.

Davis, D., Chen, G., Bandy, A., Thornton, D., Eisele, F., Mauldin, L., Tanner, D., Lenschow, D., Fuelberg, H., Huebert, B., 1999. Dimethyl sulfide oxidation in the equatorial

Pacific: comparison of model simulations with field observations for DMS, SO2, H2SO4(g), MSA(g), MS and NSS. J. Geophys. Res. 104, 5765–5784.
DeCarlo, P.F., Kimmel, J.R., Trimborn, A., Northway, M.J., Jayne, J.T., Aiken, A.C., Gonin, M., Fuhrer, K., Horvath, T., Docherty, K.S., Worsnop, D.R., Jimenez, J.L., 2006. Field-deployable, high-resolution, time-of-flight mass spectrometer. Anal. Chem. 78, 8281–8289.
Draxler, R.R., Rolph, G.D., 2003. HYSPLIT (HYbrid single-particle Lagrangian integrated trajectory) model. Available from: http://www.arl.noaa.gov/ready/hysplit4.html.
El Haddad, I., D'Anna, B., Temime-Roussel, B., Nicolas, M., Boreave, A., Favez, O., Voisin, D., Sciare, J., George, C., Jaffrezo, J.-L., Wortham, H., Marchand, N., 2013. Towards a better understanding of the origins, chemical composition and aging of oxygenated organic aerosols: case study of a Mediterranean industrialized environment, Marseille. Atmos. Chem. Phys. 13, 7875–7894.
Elser, M., Huang, R.-J., Wolf, R., Slowik, J.G., Wang, Q., Canonaco, F., Li, G., Bozzetti, C., Daellenbach, K.R., Huang, Y., Zhang, R., Li, Z., Cao, J., Baltensperger, U., El-Haddad, I., Prévôt, A.S.H., 2016. New insights into PM2.5 chemical composition and sources in two major cities in China during extreme haze events using aerosol mass spectrometry. Atmos. Chem. Phys. 16, 3207–3225.
Facchini, M.C., Decesari, S., Rinaldi, M., Carbone, C., Finessi, E., Mircea, M., Fuzzi, S., Moretti, F., Tagliavini, E., Ceburnis, D., O'Dowd, C., 2008. Important source of marine secondary organic aerosol from biogenic amines. Environ. Sci. Technol. 42, 9116–9121.
Farmer, D.K., Matsunaga, A., Docherty, K.S., Surratt, J.D., Seinfeld, J.H., Ziemann, P.J., Jimenez, J.L., 2010. Response of an aerosol mass spectrometer to organonitrates and organosulfates and implications for atmospheric chemistry. Proc. Natl. Acad. Sci. U. S. A. 107, 6670–6675.
Gondwe, M., Krol, M., Klaassen, W., Gieskes, W., de Baar, H., 2004. Comparison of modeled versus measured MSA:nss SO4 = ratios: a global analysis. Global Biochem. Cy. 18. https://doi.org/10.1029/2003GB002144.
Gramsch, E., Cereceda-Balic, F., Oyola, P., Von Baer, D., 2006. Examination of Pollution Trends in Santiago de Chile with cluster analysis of PM10 and Ozone data. Atmos. Environ. 40 (724), 5464–5475.
Gramsch, E., Reyes, R., Vásquez, Y., Oyola, P., Rubio, M.A., 2016. Prevalence of Freshly Generated Particles during Pollution Episodes in Santiago de Chile. Aerosol Air Qual. Res. 16, 2172–2185.
Hao, L.Q., Kortelainen, A., Romakkaniemi, S., Portin, H., Jaatinen, A., Leskinen, A., Komppula, M., Miettinen, P., Sueper, D., Pajunoja, A., Smith, J.N., Lehtinen, K.E.J., Worsnop, D.R., Laaksonen, A., Virtanen, A., 2014. Atmospheric submicron aerosol composition and particulate organic nitrate formation in a boreal forestland-urban mixed region. Atmos. Chem. Phys. 14, 13483–13495.
He, L.-Y., Huang, X.-F., Xue, L., Hu, M., Lin, Y., Zheng, J., Zhang, R., Zhang, Y.-H., 2011. Submicron aerosol analysis and organic source apportionment in an urban atmosphere in Pearl River Delta of China using high-resolution aerosol mass spectrometry. J. Geophys. Res. 116, D12304. https://doi.org/10.1029/2010JD014566.
Huang, X.-F., He, L.-Y., Hu, M., Canagaratna, M.R., Kroll, J.H., Ng, N.L., Zhang, Y.-H., Lin, Y., Xue, L., Sun, T.-L., Liu, X.-G., Shao, M., Jayne, J.T., Worsnop, D.R., 2011. Characterization of submicron aerosols at a rural site in Pearl River Delta of China using an aerodyne high-resolution aerosol mass spectrometer. Atmos. Chem. Phys. 11, 1865–1877.
Huang, D.D., Li, Y.J., Lee, B.P., Chan, C.K., 2015. Analysis of organic sulfur compounds in atmospheric aerosols at the HKUST supersite in Hong Kong using HR-ToFAMS. Environ. Sci. Technol. 49 3672e3679.
IPCC, 2013. Climate Change 2013: the Physical Science Basis. Cambridge University Press, Cambridge, UK and New York, NY, USA.
Kortelainen, A., Hao, L., Tiitta, P., Jaatinen, A., Miettinen, P., Kulmala, M., Smith, J.N., Laaksonen, A., Worsnop, D.R., Virtanen, A., 2017. Sources of particulate organic nitrates in the boreal forest in Finland. Boreal Environ. Res. 22, 13–26.
Koutrakis, P., Sax, S.N., Sarnat, J.A., Coull, B., Demokritou, P., Oyola, P., Garcia, J., Gramsch, E., 2005. Analysis of PM10, PM2.5 and PM10–2.5 concentrations in Santiago de Chile from 1989 to 2001. J. Air Waste Manag. Assoc. 55, 342–351.
Legrand, M., Feniet-Saigne, C., Sattzman, E.S., Germain, C., Barkov, N.I., Petrov, V.N., 1991. Ice-core record of oceanic emissions of dimethylsulphide during the last climate cycle. Nature 350, 144–146.
Lelieveld, J., Evans, J.S., Fnais, M., Giannadaki, D., Pozzer, A., 2015. The contribution of outdoor air pollution sources to premature mortality on a global scale. Nature 525, 367–371.
McGuire, M.L., Chang, R.Y.-W., Slowik, J.G., Jeong, C.-H., Healy, R.M., Lu, G., Mihele, C., Abbatt, J.P.D., Brook, J.R., Evans, G.J., 2014. Enhancing non-refractory aerosol apportionment from an urban industrial site through receptor modeling of complete high time-resolution aerosol mass spectra. Atmos. Chem. Phys. 14, 8017–8042.
Middlebrook, A.M., Bahreini, R., Jimenez, J.L., Canagaratna, M.R., 2012. Evaluation of composition-dependent collection efficiencies for the aerodyne aerosol mass spectrometer using field data. Aerosol Sci. Technol. 46, 258–271.
Ng, N.L., Canagaratna, M.R., Jimenez, J.L., Zhang, Q., Ulbrich, I.M., Worsnop, D.R., 2011. Real-time methods for estimating organic component mass concentrations from aerosol mass spectrometer data. Environ. Sci. Technol. 45, 910–916.
Onasch, T.B., Trimborn, A., Fortner, E.C., Jayne, J.T., Kok, G.L., Williams, L.R., Davidovits, P., Worsnop, D.R., 2012. Soot particle aerosol mass spectrometer: development, validation, and initial application. Aerosol Sci. Technol. 46, 804–817.
Paatero, P., Tapper, U., 1994. Positive matrix factorization – a nonnegative factor model with optimal utilization of error- estimates of data values. Environmetrics 5, 111–126.
Petzold, A., Schönlinner, M., 2004. Multi-angle absorption photometry – a new method for the measurement of aerosol light absorption and atmospheric black carbon. J. Aerosol Sci. 35, 421–441.
Saarikoski, S., Carbone, S., Decesari, S., Giulianelli, L., Angelini, F., Teinilä, K., Canagaratna, M., Ng, N.L., Trimborn, A., Facchini, M.C., Fuzzi, S., Hillamo, R., Worsnop, D., 2012. Chemical characterization of springtime submicrometer aerosol in Po Valley, Italy. Atmos. Chem. Phys. 12, 8401–8421.
Saarikoski, S., Timonen, H., Carbone, S., Kuuluvainen, H., Niemi, J.V., Kousa, A., Rönkkö, T., Worsnop, D., Hillamo, R., Pirjola, L., 2017. Investigating the chemical species in submicron particles emitted by city buses. Aerosol Sci. Technol. 51, 317–329. https://doi.org/10.1080/02786826.2016.1261992.
Salcedo, D., Laskin, A., Shutthanandan, V., Jimenez, J.-L., 2012. Feasibility of the detection of trace elements in particulate matter using online high-resolution aerosol mass spectrometry. Aerosol Sci. Technol. 46, 1187–1200.
Schmale, J., Schneider, J., Nemitz, E., Tang, Y.S., Dragosits, U., Blackall, T.D., Trathan, P.N., Phillips, G.J., Sutton, M., Braban, C.F., 2013. Sub-Antarctic marine aerosol: dominant contributions from biogenic sources. Atmos. Chem. Phys. 13, 8669–8694.
Stein, A.F., Draxler, R.R., Rolph, G.D., Stunder, B.J.B., Cohen, M.D., Ngan, F., 2015. NOAA's HYSPLIT atmospheric transport and dispersion modeling system. Bull. Am. Meteorol. Soc. 96, 2059–2077.
Sun, Y., Du, W., Wang, Q., Zhang, Q., Chen, C., Chen, Y., Chen, Z., Fu, P., Wang, Z., Gao, Z., Worsnop, D.R., 2015. Real-time characterization of aerosol particle composition above the urban canopy in Beijing: insights into the interactions between the atmospheric boundary layer and aerosol chemistry. Environ. Sci. Technol. 49, 11340–11347.
Surratt, J.D., Gómez-González, Y., Chan, A.W.H., Vermeylen, R., Shahgholi, M., Kleindienst, T.E., Edney, E.O., Offenberg, J.H., Lewandowski, M., Jaoui, M., Maenhaut, W., Claeys, M., Flagan, R.C., Seinfeld, J.H., 2008. Organosulfate formation in biogenic secondary organic aerosol. J. Phys. Chem. 112, 8345–8378.
Tagle, M., Reyes, F., Vásquez, Y., Carbone, S., Saarikoski, S., Timonen, H., Gramsch, E., Oyola, P., 2018. Spatiotemporal variation in composition of submicron particles in Santiago Metropolitan Region, Chile. Front. Environ. Sci. https://doi.org/10.3389/fenvs.2018.00027.
Tiitta, P., Leskinen, A., Hao, L., Yli-Pirilä, P., Kortelaine, M., Grigonyte, J., Tissari, J., Lamberg, H., Hartikainen, A., Kuuspalo, K., Kortelainen, A.-M., Virtanen, A., Lehtinen, K.E.J., Komppula, M., Pieber, S., Prévôt, A.S.H., Onasch, T.B., Worsnop, D.R., Czech, H., Zimmermann, R., Jokiniemi, J., Sippula, O., 2016. Transformation of logwood combustion emissions in a smog chamber: formation of secondary organic aerosol and changes in the primary organic aerosol upon daytime and nighttime aging. Atmos. Chem. Phys. 16, 13251–13269.
Timonen, H., Karjalainen, P., Saukko, E., Saarikoski, S., Aakko-Saksa, P., Simonen, P., Murtonen, T., Dal Maso, M., Kuuluvainen, H., Bloss, M., Ahlberg, E., Svenningsson, B., Pagels, J., Brune, W.H., Keskinen, J., Worsnop, D.R., Hillamo, R., Rönkkö, T., 2017. Influence of fuel ethanol content on primary emissions and secondary aerosol formation potential for a modern flex-fuel gasoline vehicle. Atmos. Chem. Phys. 17, 5311–5329.
Ulbrich, I.M., Canagaratna, M.R., Zhang, Q., Worsnop, D.R., Jimenez, J.L., 2009. Interpretation of organic components from Positive Matrix Factorization of aerosol mass spectrometric data. Atmos. Chem. Phys. 9, 2891–2918.
WHO, 2016a. Ambient air pollution: a global assessment of exposure and burden of disease. Retrieved from Geneva, Switzerland. http://www.who.int/phe/publications/air-pollution-global-assessment/en/.
WHO, 2016b. WHO releases country estimates on air pollution exposure and health impact [Press release]. Retrieved from. http://www.who.int/news-room/detail/27-09-2016-who-releases-country-estimates-on-air-pollution-exposure-and-health-impact.
Willis, M.D., Lee, A.K.Y., Onasch, T.B., Fortner, E.C., Williams, L.R., Lambe, A.T., Worsnop, D.R., Abbatt, J.P.D., 2014. Collection efficiency of the soot-particle aerosol mass spectrometer (SP-AMS) for internally mixed particulate black carbon. Atmos. Meas. Tech. 7, 4507–4516.
Zhang, Q., Alfarra, M.R., Worsnop, D.R., Allan, J.D., Coe, H., Canagaratna, M.R., Jimenez, J.L., 2005. Deconvolution and quantification of hydrocarbon-like and oxygenated organic aerosols based on aerosol mass spectrometry. Environ. Sci. Technol. 39, 4938–4952.
Zhang, Q., Jimenez, J.L., Canagaratna, M.R., Allan, J.D., Coe, H., Ulbrich, I., Alfarra, M.R., Takami, A., Middlebrook, A.M., Sun, Y.L., Dzepina, K., Dunlea, E., Docherty, K., DeCarlo, P.F., Salcedo, D., Onasch, T., Jayne, J.T., Miyoshi, T., Shimono, A., Hatakeyama, S., Takegawa, N., Kondo, Y., Schneider, J., Drewnick, F., Borrmann, S., Weimer, S., Demerjian, K., Williams, P., Bower, K., Bahreini, R., Cottrell, L., Griffin, R.J., Rautiainen, J., Sun, J.Y., Zhang, Y.M., Worsnop, D.R., 2007. Ubiquity and dominance of oxygenated species in organic aerosols in anthropogenically-influenced Northern Hemisphere midlatitudes. Geophys. Res. Lett. 34, L13801. https://doi.org/10.1029/2007GL029979.